Journal of Alloys and Compounds 1024 (2025) 180110

Contents lists available at ScienceDirect

Journal of Alloys and Compounds

journal homepage: www.elsevier.com/locate/jalcom

Creep strength of Mg-Y-Zn alloys containing long-period stacking ordered structures

Jie Wang [a], Gaoming Zhu [b,*], Dandan Wang [c], Yahui Liu [d], Xiaoqin Zeng [a,*], Marko Knezevic [e]

[a] National Engineering Research Center of Light Alloy Net Forming, Shanghai Jiao Tong University, Shanghai 200240, China
[b] Institute of Material and Process Design, Helmholtz-Zentrum Hereon, Geesthacht 21502, Germany
[c] School of Materials Science and Engineering, Changzhou University, Changzhou 213164, China
[d] School of Materials Science and Engineering, Shanghai Jiao Tong University, Shanghai 200240, China
[e] Department of Mechanical Engineering, University of New Hampshire, Durham, NH 03824, USA

ARTICLE INFO

Keywords:
Magnesium alloy
LPSO
Load transfer
High temperature creep
Stress exponent
Activation energy

ABSTRACT

Magnesium (Mg) alloys reinforced with long-period stacking ordered (LPSO) structures exhibit considerable potential for achieving enhanced mechanical properties. Despite progress in understanding tensile and compressive deformation mechanisms at elevated temperatures, the comprehension of the creep behavior of these alloys under varying conditions remains incomplete. The present study investigates the creep behavior of three Mg-Y-Zn alloys containing varying contents of LPSO structures under different temperature and stress conditions. The findings reveal that at 150 °C, the LPSO phase content has an insignificant effect on the creep resistance of the alloys. However, as temperature exceeds 200 °C, the creep resistance deteriorates with increasing LPSO phase content. Notably, at higher temperatures (300 °C), the alloys exhibit superplasticity during creep deformation, which is attributed to the diffusion of solute atoms facilitated through stacking faults within the LPSO structures. A creep constitutive equation was developed for temperatures between 150℃ and 200 ℃ and stress levels of 170–230 MPa, revealing high stress exponents (n = 7.1–8.6) and low activation energies (Q_c=80.98–90.63 kJ·mol^{-1}) for the alloys. These results align with power-law dislocation creep, indicating threshold stress fields resulting from load transfer between the α-Mg matrix and the LPSO phase. After adjustment for the threshold stress, the stress exponents imply diffusional creep as the primary mechanism. The findings in this research contribute to understanding creep mechanisms in these alloys and offer insights into optimizing their performance for diverse applications.

1. Introduction

Magnesium (Mg) alloys have gained significant attention in industries such as automotive, railway and aerospace due to their excellent strength-to-weight ratio, making them ideal for lightweight structural applications [1,2]. However, their widespread use has been limited by poor creep resistance in high-temperature applications, which remains a critical challenge [3]. The creep properties of Mg alloys are influenced by various factors, including grain size [4], alloying elements [5], phases [6], and their morphological characteristics [7]. Understanding these factors is essential for improving the performance of Mg alloys under high-temperature and stress conditions.

One promising approach to enhancing creep resistance of Mg alloys is the addition of rare-earth (RE) elements [8]. Solid solution strengthening and dynamic precipitation strengthening are two key mechanisms that have shown potential in improving the creep performance of Mg alloys. For instance, a study has demonstrated that binary Mg-RE alloys exhibit improved high-temperature mechanical properties due to the short-range ordered strengthening effect [9]. Similarly, another study investigated the role of Gd solutes in extruded Mg-Gd alloy, revealing that interactions between dislocations and RE atoms enhance creep resistance by forming dislocation structures and promoting dynamic precipitation [10].

Another effective strategy involves integrating thermally stable phases into the alloy, such as long-period stacking ordered (LPSO) structures, into Mg-RE-Zn alloys. These LPSO structures are known for their exceptional mechanical properties across a range of temperatures [11–13]. In Mg alloys with LPSO phases, the material exhibits high stress

* Corresponding authors.
E-mail addresses: gaoming.zhu@hereon.de (G. Zhu), xqzeng@sjtu.edu.cn (X. Zeng).

https://doi.org/10.1016/j.jallcom.2025.180110
Received 11 September 2024; Received in revised form 23 March 2025; Accepted 29 March 2025
Available online 4 April 2025

exponents and activation energies, particularly at low temperatures and high strain rates [14]. The improved creep resistance is attributed to the ability of the LPSO phase to bear loads, similar to reinforcement in metal matrix composites. For example, Garcés et al., studied the creep resistance of a $Mg_{97}Y_2Zn_1$ (at%) alloy containing 18 R and 14H-LPSO structures at temperatures ranging from 200 ℃ to 350 ℃ [15]. They found that the 14H-LPSO structure outperformed the 18R-LPSO variant at low temperatures and high strain rates, acting as a barrier within the α-Mg grains to resist deformation. On the other hand, at higher temperatures and lower strain rates, the 18R-LPSO demonstrated better creep resistance by hindering the movement of dislocations through solute atoms. These findings highlight the superior creep resistance of LPSO-reinforced Mg alloys compared to other Mg-RE alloys [8].

Despite these advancements, the relationship between LPSO phase content and creep resistance remains poorly understood. While the studies have shown a positive correlation between increased LPSO content and enhanced creep resistance, the underlying mechanisms are not fully elucidated [16]. Recent research has demonstrated that optimizing the microstructure through heat treatment can significantly improve creep resistance in α-Mg/LPSO duplex Mg-Y-Zn alloys [17]. However, a deeper understanding of the factors governing creep behavior in LPSO-containing Mg alloys is necessary to guide the design of microstructures and developing alloys with superior performance.

In this study, we investigate the creep characteristics of extruded Mg-LPSO dual-phase alloys, focusing on the influence of LPSO phase content, temperature, and applied stress levels. Additionally, we develop a creep constitutive equation to provide insights into the creep properties of these alloys. By elucidating the mechanisms underlying creep resistance, this work aims to contribute to the development of Mg alloys with enhanced performance for high-temperature applications.

2. Experimental procedures

2.1. Materials

To prepare the Mg-Y-Zn alloys, pure Mg (99.95 wt%), pure Zn (99.99 wt%), and Mg-25 wt%Y master alloys were used as raw materials. During melting of the alloys, a protective atmosphere comprising 1.0 vol% SF_6 and 99.0 vol% CO_2 was used to prevent oxidation. The melt was kept at 750 ℃ for 30 mins to ensure a uniform composition, then gradually cooled to 725 ℃ before being poured into a preheated cylindrical steel mold [18]. Billets with different alloying contents were cast through this process. The chemical compositions of the three cast billets were analyzed using inductively coupled plasma atomic emission spectroscopy (ICP-AES), as shown in Table 1. The as-cast alloys were subjected to homogenization at 400 ℃ for 24 hours. Hot extrusion was conducted at the same temperature. This step was carried out with an extrusion speed of 2 $mm{\cdot}s^{-1}$, producing round bars with a diameter of 14 mm, corresponding to an extrusion ratio of 18:1.

2.2. Creep tests

The creep tests were conducted using a WinCCS-controlled lever arm tester (model # 2320-MM) manufactured by Applied Test Systems (ATS). The testing machine comprises an extensometer frame (Series 4124 A), a load train consisting of two series 4043 pull rods and two series 4031 A threaded couplings, and two displacement encoders (left and right). Additionally, the machine features a thermocouple junction where two K-type thermocouples (top and bottom) are connected. The samples were prepared in accordance with the ASTM E606M standard, as shown in Fig. 1. The samples were gradually heated to the specified temperatures for ~1 hour and held at each temperature for 0.5 hours. Five temperatures were selected for the creep testing: 150 °C, 175 °C, 200 °C, 250 °C, and 300 °C. Manual intervention was employed for some tests to halt the process within the secondary region, allowing the extraction of creep parameters for use with the Mukherjee-Bird-Dorn Equation [19].

Table 1
Chemical compositions (in wt%) of the Mg-Y-Zn alloys analyzed by ICP-AES.

Alloys	Elements						
	Y	Zn	Mn	Cu	Ni	Fe	Mg
Y1	1.714	1.391	0.0124	0.0071	0.0016	0.0159	Bal.
Y2	8.805	2.856	0.0130	0.0019	0.0030	0.0293	Bal.
Y4	11.270	4.865	0.1156	0.0013	0.0357	0.0154	Bal.

2.3. Electron microscopy and synchrotron X-ray diffraction

Microstructures of the alloy were characterized using scanning electron microscopy (SEM) and electron backscattered diffraction (EBSD) with a MIRA 3 LHM, TESCAN instrument. Sample surfaces were first mechanically ground with sandpaper, then electro-polished in an ethanol solution containing 10 % perchloric acid electrolyte for SEM and EBSD experiments. Electro-polishing was performed under conditions of 30 V and 0.5 A at a temperature of −35 ^{0}C for 150 s. EBSD measurements were carried out at an accelerating voltage of 20 kV with a scan step size of 500 nm. The acquired EBSD data were processed using TSL OIM Analysis 7 software (EDAX Inc). To investigate finer microstructures, transmission electron microscopy (TEM) was employed using a JEOL JEM-2100F microscope. TEM samples were prepared by twin-jet electropolishing in a 4 % perchloric acid-ethanol solution at 30 V and −40 ^{0}C, followed by ion milling for further refinement. Additionally, synchrotron X-ray diffraction experiments were conducted at beamline P21.2 of Deutsches Elektronen-Synchrotron (DESY) with an energy of 82 keV. The beam size was set to 500 × 500 μm^2, enabling the examination of a larger volume (0.25 cm^3). Diffraction patterns were analyzed using the open-source software pyFAI (https://github.com/kif/pyFAI).

3. Results

3.1. Initial microstructure

The microstructure of the three alloys consists of LPSO phase and α-Mg grains. As illustrated in Fig. 2(a-f), the secondary electron (SE) images and image quality (IQ) maps display the features of the extruded Mg-Y-Zn alloys. The SE images demonstrate the fibrous alignment of the LPSO phase along the extrusion direction (ED), while the IQ maps reveal that the α-Mg grains underwent complete dynamic recrystallization (DRX) during hot extrusion. The average grain sizes of α-Mg in the Y1, Y2, and Y4 alloys were measured as 6.6 ± 2.3 μm, 4.4 ± 1.5 μm, and 3.0 ± 1.2 μm, respectively. The corresponding area fractions of the LPSO phase, measured as 4.5 ± 0.8 % for Y1 alloy, 27.3 ± 0.5 % for Y2 alloy, and 49.8 ± 1.1 % for Y4 alloy, respectively. Two-dimensional (2D) X-ray diffraction patterns and one-dimensional (1D) X-ray diffraction profiles were shown in Fig. 2(g, h), revealing polycrystalline materials [20]. The diffraction peaks were identified as belonging to the LPSO phase and Mg phase, consistent with the microstructures presented in Fig. 2(a-f).

To further investigate the microstructure of the Y2 alloy, bright field (BF) image was recorded as shown in Fig. 3(a), demonstrating a "sandwiched structure" where LPSO phases are interspersed with Mg matrix. The representative selected area electron diffraction (SAED) pattern confirms the LPSO phase with 18R-type stacking sequence, consistent with prior studies on alloys with similar compositions [11,12,21]. In addition, the α-Mg matrix contains numerous stacking faults (SFs), as illustrated in the BF image in Fig. 3(b). The corresponding SAED pattern indicates that these SFs were formed on the {0002} planes. Such microstructure features have implications for the creep performance, which will be discussed in later sections.

In a previous study, we evaluated the thermal stability of the LPSO phase and α-Mg phase in a Mg-Y-Zn alloy using differential scanning

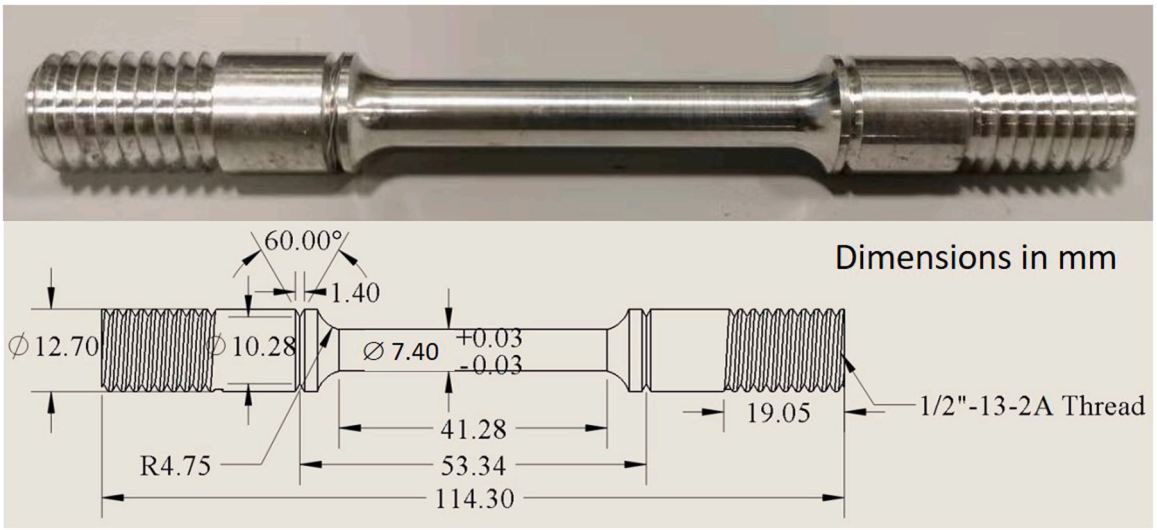

Fig. 1. Creep specimen following the American Society for Testing and Materials (ASTM) E606M standard.

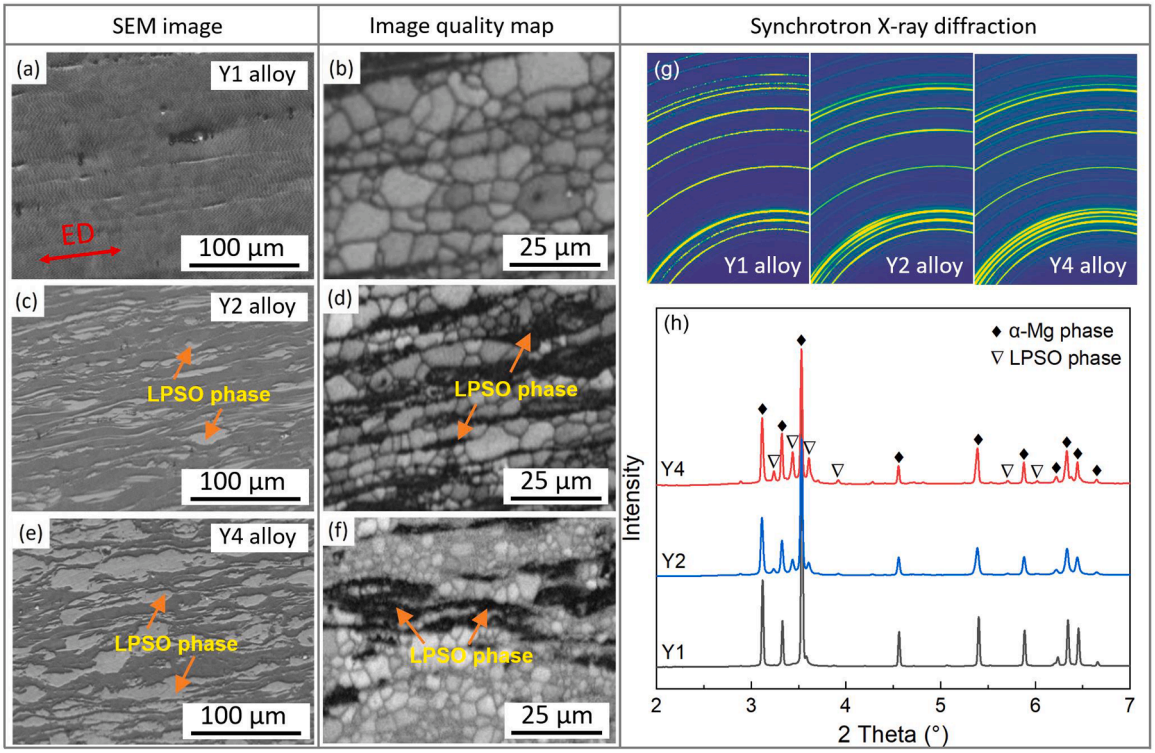

Fig. 2. Secondary electron images ((a), (c), and (e)), image quality (IQ) maps ((b), (d), and (f)), synchrotron X-ray diffraction patterns (g), and the 1D X-ray diffraction profiles (h) of the three Mg-Y-Zn alloys, showing the grain structure, phase constitution, and phase content of the alloys.

calorimetry (DSC) analysis [12]. The results revealed that the dissolution temperatures of the LPSO phase and α-Mg phase are 536.5 °C and 628.4 °C, respectively. According to the creep criterion [22], the critical temperature for high-temperature creep in the α-Mg phase is approximately 204.7 °C, while for the LPSO phase, it is around 161 °C.

3.2. *Effect of LPSO content on creep deformation at 150 °C*

Fig. 4 presents the creep curves of the Y1, Y2, and Y4 alloys at the temperature of 150 °C and an applied stress of 170 MPa. It is evident from the curves that the specimens initially exhibit instantaneous strain, primarily composed of elastic strain, when the applied stress is below the yield stress. Subsequently, the alloys undergo time-dependent creep deformation. The complete creep deformation can be divided into three stages. During the primary creep stage, known as the deceleration creep or transitional creep stage, the Y1 alloy exhibits the highest creep strain rate ($d\varepsilon/dt$), while the Y4 alloy demonstrates the lowest. Based on the analysis of high-temperature tensile deformation in a Mg-LPSO alloy, it was observed that the LPSO phase plays a significant role in strengthening the material when deformed below 200 °C [12]. Moreover, the size of the LPSO phase surpasses that of the α-Mg grains, and the main strengthening mechanism is load transfer in these bulk fiber-reinforced alloys [23]. The harder LPSO phases bear a greater portion of the load, thus reducing the load on the α-Mg matrix. As a result, the creep rates of

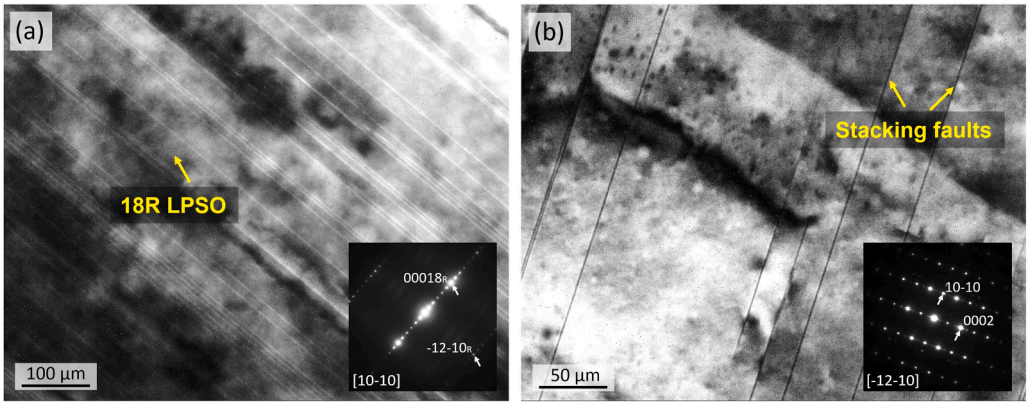

Fig. 3. TEM bright field (BF) micrographs of (a) LPSO structure and (b) stacking faults (SFs) in the as-extruded Y2 alloy. The insets are representative selected area electron diffraction (SAED) patterns showing the LPSO with a 18 R type structure. The SFs were formed on the basal planes of Mg.

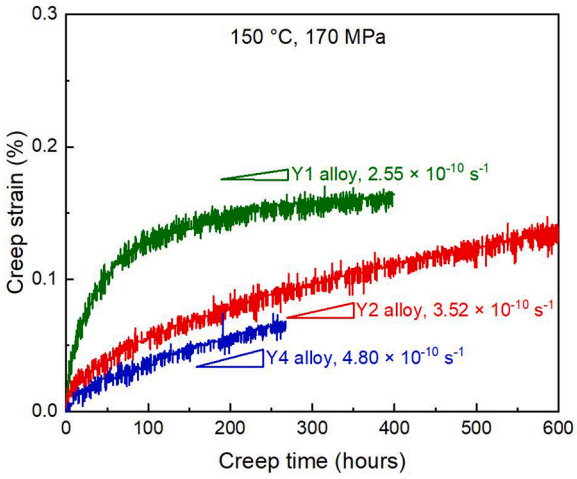

Fig. 4. Typical creep curves of the Y1, Y2, and Y4 alloys at the temperature of 150 °C and the applied stress of 170 MPa.

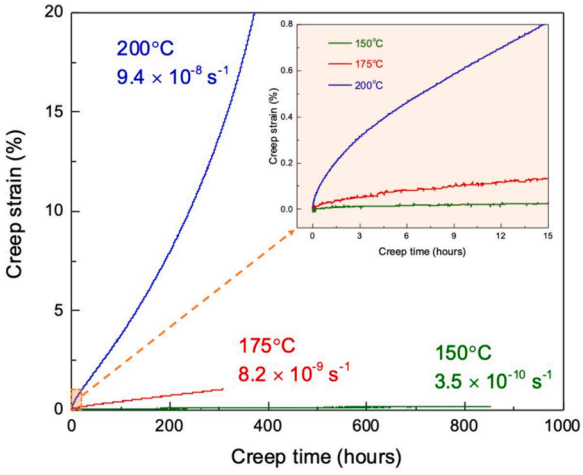

Fig. 5. Typical creep curves of the Y2 alloy under the stress of 170 MPa and at different temperatures.

the high content LPSO-containing Mg alloys in the first stage are lower than those of the low content LPSO-containing Mg alloys.

The secondary creep stage deformation is known as the steady-state creep stage. At 150 °C, the content of the LPSO phase has a small effect on the creep rate of the alloy during this stage. The steady creep rates of all three alloys are on the order of $10^{-10}\ s^{-1}$. The Y1 alloy exhibited the lowest creep rate of $2.55 \times 10^{-10}\ s^{-1}$, while the Y4 alloy demonstrated the highest creep rate of $4.80 \times 10^{-10}\ s^{-1}$. It can be inferred that increasing the volume fraction of LPSO phase has an insignificant effect on the creep performance of the alloys at the temperature around 150 °C (T/Tm ≈ 0.2, Tm is the melting temperature). During the creep deformation, changes in properties such as hardness, elastic modulus, and internal friction occur over time, indicating alterations in the microstructure. Dislocation slip is an important mechanism throughout the entire creep deformation, particularly at lower temperatures and under higher stress conditions.

3.3. Temperature-dependent creep deformation

The creep behavior of the LPSO Mg alloy exhibited noticeable variations as the temperature changed under a specific applied stress. Fig. 5 shows the creep curves of the Y2 alloy at different temperatures while being subjected to a stress of 170 MPa. An increase in temperature from 150 °C to 175 °C resulted in a substantial elevation in the steady-state creep rate of the alloy. Specifically, the creep rate increased from $3.5 \times 10^{-10}\ s^{-1}$ to $8.2 \times 10^{-9}\ s^{-1}$. Moreover, at 200 °C, the secondary creep stage was significantly shortened, with the creep rate continuing to exponentially rise to $9.4 \times 10^{-8}\ s^{-1}$. This substantial increase in the creep rate demonstrates the strong temperature dependence of the alloy's creep behavior.

Steady-state creep deformation arises from the dynamic equilibrium between work hardening and recovery softening. From the dislocation perspective, it represents a balance between dislocation multiplication through slip and dislocation annihilation through climb. The results of this study reveal a linear correlation between the logarithm (log) of the steady-state creep rate and the reciprocal of the absolute temperature (T^{-1}), as shown in Fig. 6. This relationship between the steady-state creep rate and temperature can be mathematically expressed as follows [24]:

$$\dot{\varepsilon} = A_1 * \exp\left(\frac{-Q_c}{RT}\right) \quad (1)$$

Where

A_1 is a constant associated with stress and material properties,

R is the gas constant (8.3145 $J{\cdot}mol^{-1}{\cdot}K^{-1}$),

T is the absolute temperature,

Q_c is the apparent activation energy.

The apparent activation energy (Q_c) was determined to be 80.98 $kJ{\cdot}mol^{-1}$ from the slope of the linear relationship, as shown in Fig. 6.

During steady-state creep deformation, the dislocation substructure is determined by the normalized shear modulus stress and remains in-

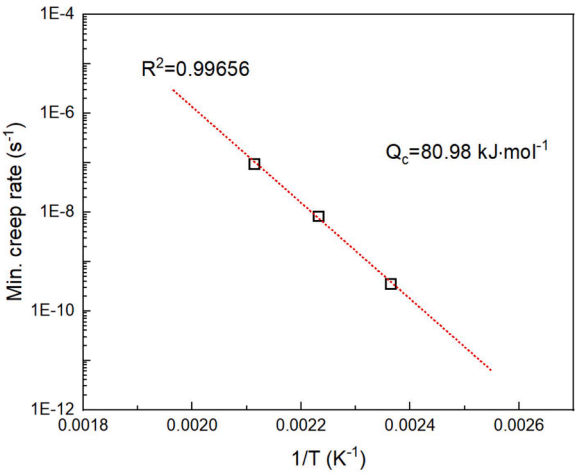

Fig. 6. The relationship between minimum creep rate and temperature for Y2 alloy under the stress of 170 MPa.

dependent of temperature. The creep activation energy reflects how the creep rate changes with temperature under a specific stress and dislocation substructure. Extensive experimental observations indicate a strong resemblance between the creep activation energy Q_c and the activation energy for self-diffusion Q_{sd}, indicating a significant correlation between the creep and diffusion processes [25]. Recent studies further demonstrated that the addition of solute atoms modifies both the self-diffusion activation energy and the creep activation energy, while still satisfying the equation $Q_c = Q_{sd}$ [26]. As dislocation climb involves atomic diffusion, power-law creep is governed by the diffusion process. The relationship between the activation energy for diffusion and the diffusion coefficient of elements can be determined using the Arrhenius equation:

$$D_{a/c-axis}^{Mg/Zn/Y} = D_0 \cdot \exp(-Q/RT) \quad (2)$$

Where

D is the diffusion coefficient,

D_0 is the diffusion constant,

Q is the diffusion activation energy,

R is the gas constant,

T is the absolute temperature.

The self-diffusion activation energy of Mg falls within the range of 137.979–138.943 kJ·mol^{-1} [27]. On the other hand, the diffusion activation energies of the solute elements zinc (Zn) and yttrium (Y) in Mg range from 132.725 to 135.488 kJ·mol^{-1} and 97.852–99.127 kJ·mol^{-1}, respectively [28,29], as shown in Table 2. The Y2 alloy exhibits a relatively low creep activation energy of 80.98 kJ·mol^{-1}, which is lower than the diffusion activation energy of any individual constituent element in the alloy.

As mentioned previously, the steady-state creep rate is influenced not only by the material itself but also by two external variables: temperature (T) and stress (σ). By conducting orthogonal creep experiments at different temperatures and under various applied stresses, it is possible to establish the relationship among the steady-state creep rate, temperature, and stress, thereby obtaining the creep constitutive equation. Table 3 presents the creep results of Mg-LPSO alloys subjected to various temperatures and applied stresses. In most experiments, the tests were manually stopped when the specimen entered into the steady-state creep stage or when the extensometer reached its limit (~25 % strain). As a result, the creep curves do not provide a comprehensive representation of the complete creep deformation process. Moreover, Mg-LPSO alloys demonstrated favorable high-temperature creep deformation capabilities, often exceeding 100 % strain, which is why there is scarce information available regarding the exact time of creep fracture occurrence in these specimens.

Table 2
Pre-exponential factor D_0 and activation energy of Mg, Zn, and Y in Mg.

	Pre-exponential factor Do (m^2·s^{-1})	Activation energy Q (kJ·mol^{-1})
D_{a-axis}^{Mg}	1.75×10^{-4}	137.979
D_{c-axis}^{Mg}	1.78×10^{-4}	138.943
D_{a-axis}^{Zn}	4.98×10^{-5}	132.725
D_{c-axis}^{Zn}	7.33×10^{-5}	135.488
D_{a-axis}^{Y}	2.79×10^{-8}	97.852
D_{c-axis}^{Y}	3.21×10^{-8}	99.127

3.4. Effect of LPSO content on creep deformation at 300 °C

As the applied stress or temperature increases, the secondary creep stage of creep shortens or even disappears, directly entering into the tertiary creep stage. This stage is known as the accelerating creep stage, where the creep rate gradually increases with time until fracture. Fig. 7 illustrates the creep curves and creep rate over time for the three alloys at a temperature of 300 °C ($T/T_m \cong 0.43$). Under certain stress levels, the Y1 alloy exhibited the lowest creep rate, followed by the Y2 alloy, while the Y4 alloy exhibited the highest creep rate. This suggests that alloys with a higher LPSO phase content exhibit poorer creep resistance. When the applied stress increased from 50 MPa to 80 MPa, the creep rate of all three alloys significantly increased throughout the creep deformation. However, compared with 150 °C, the secondary creep stage was considerably shortened at 300 °C when a stress of 50 MPa was applied, and disappeared under 80 MPa. Furthermore, the higher the content of the LPSO phase, the faster the alloy entered into the tertiary creep stage at 300 °C, and the higher the creep rate throughout the entire creep deformation.

High-temperature creep deformation involves both intragranular deformation and grain boundary sliding. In the case of fine-grained materials, the influence of grain size on creep rate cannot be neglected, as the contribution of diffusion creep increases with decreasing grain size. In general, smaller grain sizes result in higher creep rates in alloys. However, despite the Y4 alloy having the smallest grain size (~3.0 μm), the α-Mg grains only accounted for 50.2 % of the alloy. On the other hand, the Y1 alloy had the largest grain size (~6.4 μm), but the α-Mg grains accounted for 95.5 %. The number of α-Mg grain boundaries in the Y1 alloy is much higher than that in the Y4 alloy. Therefore, the poor creep resistance of alloys with a high LPSO phase content cannot be solely attributed to smaller grain size of α-Mg.

During creep testing at 300 °C, the alloys displayed creep strain exceeding 100 % (see Fig. S1 in Supporting Information). Achieving

Table 3
Creep properties of the three LPSO-containing Mg-Y-Zn alloys at different temperatures and stresses.

Alloy	Temperature (°C)	Stress (MPa)	Minimum creep rate (s^{-1})	Run time (hours)	Creep strain (%)
Y1	150	170	2.55×10^{-10}	396	> 0.47
Y1	300	50	2.05×10^{-6}	12	> 18.8
Y2	150	170	3.52×10^{-10}	852	> 0.175
Y2	150	200	6.22×10^{-10}	1374	> 0.56
Y2	150	230	2.86×10^{-9}	182	> 0.36
Y2	175	170	8.21×10^{-9}	308	> 1.039
Y2	175	200	1.94×10^{-8}	716	> 5.5
Y2	175	230	7.58×10^{-8}	33	> 1.369
Y2	200	170	9.44×10^{-8}	415	> 25
Y2	200	200	3.24×10^{-7}	136	> 25
Y2	200	230	1.24×10^{-6}	35	> 25
Y2	250	170	1.72×10^{-5}	3	> 25
Y2	300	50	9.48×10^{-6}	3.6	> 16.7
Y4	150	170	4.80×10^{-10}	267	> 0.068
Y4	300	50	1.62×10^{-5}	3	> 25

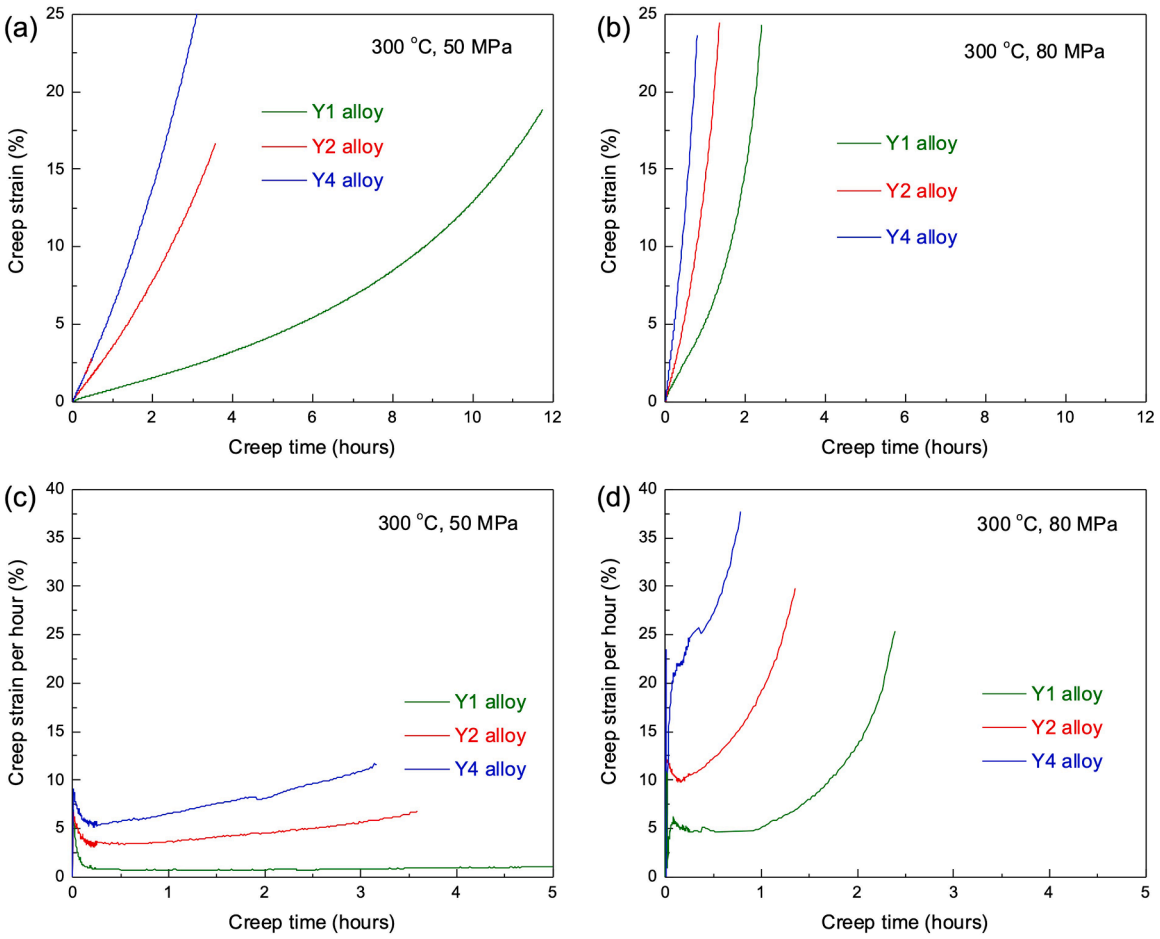

Fig. 7. Typical creep curves of the Y1, Y2, and Y4 alloys at the temperature of 300 °C and stresses of (a) 50 MPa and (b) 80 MPa, creep rate as a function of creep time at applied stresses of (c) 50 MPa and (d) 80 MPa.

superplasticity in metals typically necessitates high temperatures ($T \geq 0.5\ T_m$), low deformation rates ($\varepsilon \leq 0.001\ s^{-1}$), and the presence of fine, equiaxed grains (< 10 μm). It is crucial to maintain micrometer-sized, fine grains throughout the entire deformation process. Fig. 8 shows the microstructure of a creep-fractured Y2 alloy at 300 °C, revealing extensively fragmented LPSO phases and fine dynamically recrystallized (DRXed) α-Mg grains in the crept sample. The LPSO phase plays a significant role in this regard, as its presence and fragmentation during deformation act as pinning agents for grain boundaries, effectively restraining grain growth and stabilizing the grain size. Moreover, the occurrence of superplastic deformation is influenced by the relative stress between the matrix and the secondary phase. When there is a significant load partition between the two phases, stress concentration often arises at the interface, leading to void formation and premature fracture. However, in our previous study [12], it was observed that LPSO and α-Mg exhibit comparable lattice strain under deformation at 300 °C, indicating a balanced stress distribution. This equilibrium effectively minimizes stress concentration at the phase boundaries, thereby enhancing the superplastic deformation capability of Mg-LPSO alloys during high-temperature creep.

At elevated temperatures and low applied stresses, the creep rate exhibits a positive correlation with stress. This type of creep deformation is influenced not only by dislocation behavior but also by the phenomenon of diffusion creep, which involves the directional flow of substances under stress [30]. Fig. 9 presents a schematic diagram illustrating the diffusion creep mechanism in both Mg and the LPSO

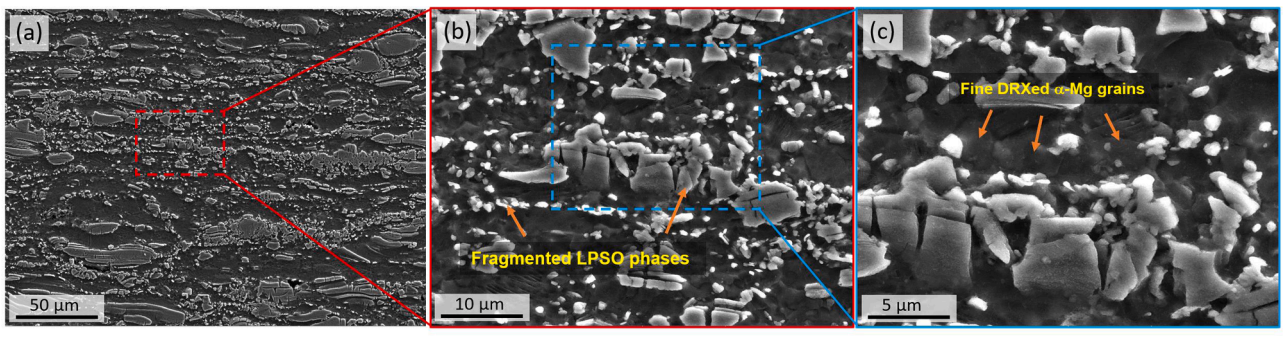

Fig. 8. Secondary electron images of the Y2 alloy after creep fracture at 300 °C under stress of 50 MPa.

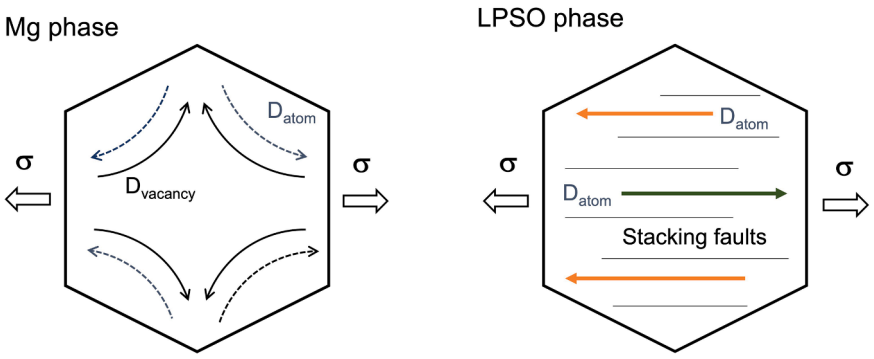

Fig. 9. Schematic of diffusion mechanisms for Mg and LPSO phase in creep.

phases. When an alloy is subjected to constant stress, the energy required for vacancy formation around the grain boundary, where tensile stress is applied, is relatively low. Over time, the concentration of vacancies increases in this region. Conversely, areas of the grain boundary experiencing compressive stress have lower vacancy concentrations. Consequently, a vacancy concentration gradient forms within the crystals, causing vacancies to migrate from regions of high concentration to regions of low concentration. This migration of vacancies results in atomic diffusion in the opposite direction, leading to grain deformation along the loading direction. The LPSO structure, with its abundance of stacking faults, provides rapid diffusion channels for solute atoms, in addition to relying on the concentration gradient of vacancies [31]. Additionally, at elevated temperatures, the weakened strength of grain boundaries allows for their sliding and migration under loading, contributing to creep deformation. However, the significant contribution of grain boundary sliding to creep elongation is primarily observed at relatively high temperatures and low deformation rates.

To quantitatively describe the influence of the LPSO phase on the different stages of creep deformation in the alloys, the average creep rate was calculated at various creep strain intervals. Fig. 10(a) presents the average creep rate of the Y1, Y2, and Y4 alloys at different stages of creep deformation under an applied stress of 80 MPa and at a temperature of 300 °C. In the case of the Y1 alloy, the creep rate exhibited an acceleration as the creep deformation progressed. However, as the content of the LPSO phase increased, the differences in creep rates between the various stages of creep deformation narrowed. Although the LPSO phase contributed to an overall acceleration in the creep rate, its impact on the later stage of creep (the tertiary creep stage) was relatively smaller compared to the earlier stage (the secondary creep stage). Although the LPSO phase exhibited a detrimental effect on creep resistance at high temperatures (the secondary creep stage), it played a stabilizing role in the tertiary stage of creep deformation. This stabilization mechanism can be beneficial in preventing catastrophic fracture failure.

Upon comparing the creep curves of Mg-Y-Zn alloys with varying contents of the LPSO phase under specific temperature and stress conditions, it becomes evident that the presence of the LPSO phase contributes to poor creep resistance in these alloys. Fig. 10(b) illustrates the increase in the average creep rate at different creep stages as the applied stress increases from 50 MPa to 80 MPa. It can be found that with a certain increase in applied stress (30 MPa), the increment of creep rate throughout the entire creep deformation shows an accelerating trend as the increase in the content of the LPSO phase increases. In the case of the Y1 alloy, an increase in applied stress leads to a noticeable acceleration in the creep rate. For the Y4 alloy, the same increase in applied stress results in a similar initial increase in the creep rate (<10 % strain), followed by a more pronounced acceleration in the later stage (>10 % strain). Comparatively, the creep behavior of the LPSO Mg alloy exhibits greater sensitivity to the applied stress at 300 °C.

4. Discussion

In this research, a temperature range of 150–300 °C was selected. In order to obtain a comprehensive creep curve, a stress range of 170–230 MPa was chosen. Fig. 11 illustrates the creep curves of the Y2 alloy at different temperatures and varying applied stresses. Both temperature and stress increase contributed to an elevation in the creep rate. During the initial stage of creep, also known as the first stage, the creep rate exhibited rapid growth, indicating low deformation resistance. However, as creep deformation progressed, work hardening occurred, gradually reducing the creep rate with increasing creep time. Simultaneously, the dynamic recovery rate gradually increased alongside the growing work hardening. Eventually, a dynamic equilibrium was achieved between these two processes, which is observable as a constant

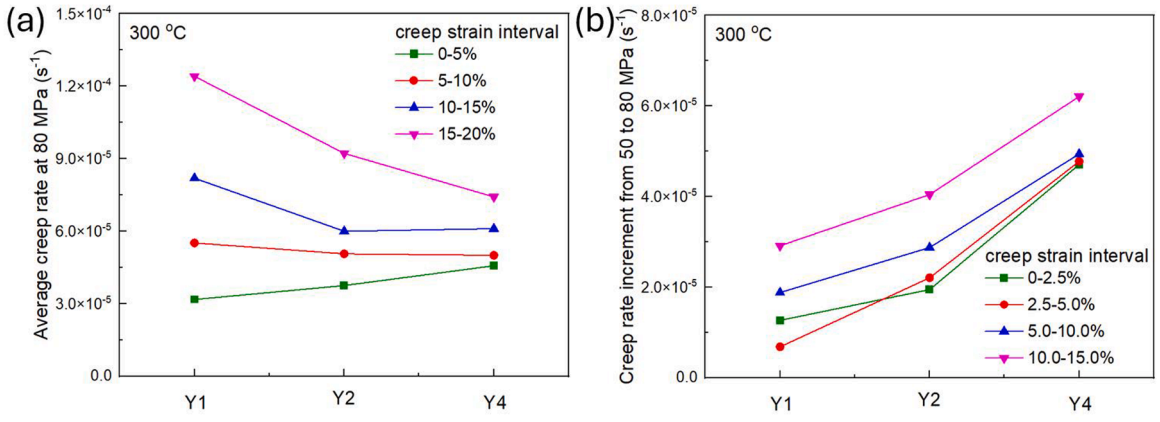

Fig. 10. (a) Average creep rate at 80 MPa and (b) creep rate increment from 50 MPa to 80 MPa for Y1, Y2, and Y4 alloys at different creep strain intervals at 300 °C.

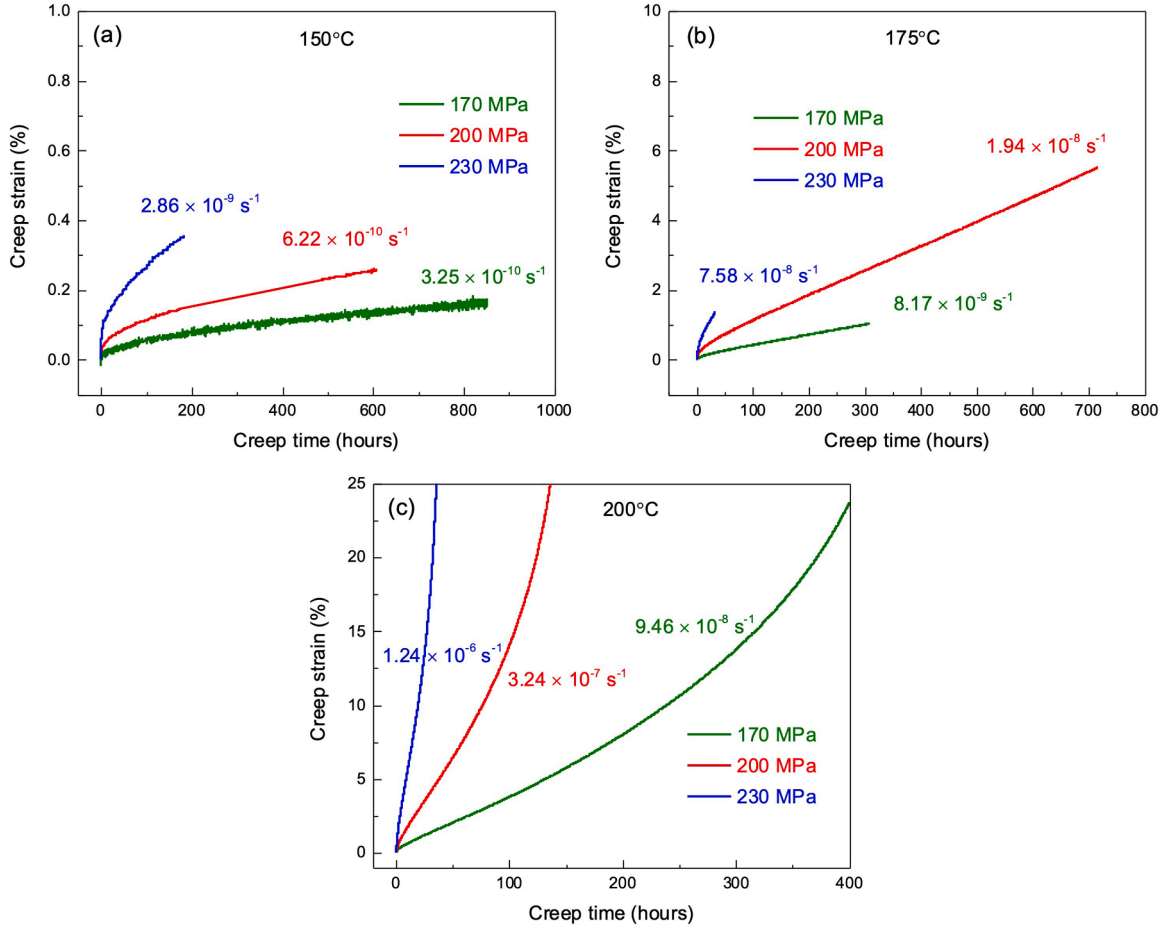

Fig. 11. Typical creep curves of the Y2 alloy under different stresses at the temperatures of (a) 150 °C, (b) 175 °C, and (c) 200 °C.

creep rate. This marks the onset of the secondary creep stage of creep deformation, referred to as steady-state creep. The steady-state creep rate is commonly utilized as an indicator to evaluate the creep resistance performance of materials.

The activation energy (Q) value for creep provides more precise insights into the creep mechanism. Fig. 12 illustrates the relationship between the steady-state creep rate and temperature of the Y2 alloy under different applied stresses. By utilizing Eq. (1), we calculated the creep activation energy to be in the range of 80.98–90.63 kJ·mol^{-1} for applied stresses ranging from 170 to 230 MPa. These values were found to be lower than the diffusion activation energy of Mg and the solute atom Zn but close to that of the solute atom Y. The mechanism of creep deformation depends on both stress and temperature. At high temperatures and low stresses, diffusion creep becomes the primary mechanism governing the creep rate [32]. Depending on the diffusion paths, lattice diffusion occurs at higher temperatures ($T > 0.7Tm$, where Qc ≈ 135 kJ·mol^{-1}), while grain boundary diffusion occurs at lower temperatures (T ≈ 0.4–0.7Tm, where Qc ≈ 60–80 kJ·mol^{-1}). Under moderate temperatures and stresses, creep deformation is mainly dominated by dislocation behavior [33]. The activation energy for creep dominated by dislocation climb is typically around 135 kJ·mol^{-1}, whereas for creep dominated by dislocation cross slip, it is higher, generally exceeding 200 kJ·mol^{-1}. In the case of creep dominated by pipeline diffusion, the activation energy is around 92 kJ·mol^{-1} [34,35].

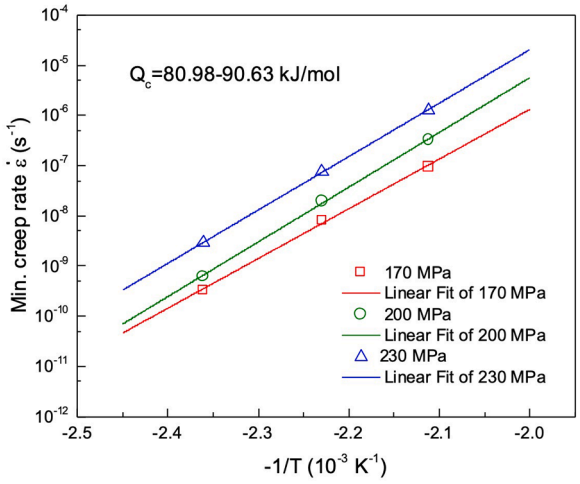

Fig. 12. The relationship between minimum creep rate and temperature for Y2 alloy under different stresses.

The obtained Q value in this study closely aligns with the activation energy for atomic pipeline diffusion, which involves the diffusion of atoms through dislocation cores. As a result, pipeline diffusion and the diffusion of Y atoms were identified as the mechanisms controlling the creep rate. Luthy et al. [36] proposed that when the diffusion activation energy of dislocation channels is similar to the creep activation energy, dislocation climb still governs creep deformation. However, due to the high applied stress, the dislocation density within the material is also high, allowing the dislocation climb process to occur through dislocation diffusion channels rather than relying on bulk diffusion. Some studies [37,38] have also observed that the creep activation energy at low temperatures is comparable to the activation energy for cross slip, leading to the belief that dislocation cross slip or dislocation cutting by

slip dislocation controls the creep rate. The addition of the rare earth element Y can reduce the stacking fault energy of the Mg alloy [39]. A significant number of stacking faults were observed in the alloys, which can persist during deformation at 200 °C [12]. In alloys with low stacking fault energies, cross slip is less likely to occur due to the wider width of dislocation propagation. It is possible that stacking faults may influence the rate of dislocation climb.

A large number of experimental results demonstrate a linear relationship between the logarithm of steady-state creep rate (ε_s) and the logarithm of applied stress (σ) [40,41]. This observation suggests that the creep behavior of alloys typically adheres to power-law creep. The temperature and stress effects are commonly expressed using the following equation:

$$\frac{\varepsilon_s kT}{DGb} = A\left(\frac{\sigma}{G}\right)^n \tag{3}$$

Where

A is a constant that is associated with material properties and temperature,

D denotes the self-diffusion coefficient,

G is the shear modulus (16.7 GPa),

b is the dislocation Burger vector,

k is the Boltzmann constant,

n is the stress exponent of the steady-state creep rate.

The stress exponent (n) can be determined from the slope of the line on the logarithmic scale. This Eq. (3) represents the relationship among creep rate, stress, and temperature and is commonly referred to as the creep constitutive equation or creep equation. In addition to the creep activation energy (Qc), the value of the stress exponent (n) can also provide insights into the creep deformation mechanisms. Fig. 13(a) illustrates the relationship between the steady-state creep rate and stress for the Y2 alloy. It is evident that the steady-state creep rate exhibits a high stress exponent, ranging from 7.1 to 8.6 within the temperature range of 150 °C to 200 °C.

The primary creep mechanisms observed in most Mg alloys are dislocation creep ($n \approx 5$) and grain boundary diffusion ($n \approx 1$). However, studies have also identified certain Mg alloys with high stress exponent ($n > 5$) that do not conform to power-law creep behavior. This phenomenon can be attributed to the presence of a threshold stress, which arises from the interaction between dislocations and precipitates, reinforcements, or dispersoids. Maruyama et al. [3] reported a stress exponent value of approximately 12 for the Mg-Y binary alloy, which they attributed to dislocation detachment from the solute atmosphere under external stress. Zhu et al. [42] associated stress exponents in the range of 6–9 observed in Mg-RE alloys with dislocation creep. They observed dynamic precipitation and proposed that the precipitated phase acted as an effective barrier against dislocation motion.

Furthermore, in metal matrix composites or alloys reinforced with particles or fibers, high stress exponents are often linked to the threshold stress generated by the reinforcements. Garces et al. [15] recently correlated the high stress exponent ($n = 11$) in the $Mg_{97}Y_2Zn_1$ alloy with the hard LPSO phases present in the alloy. They suggested that the LPSO phase could serve as a reinforcing fiber, effectively bearing loads during deformation and inducing the generation of threshold stress in dislocations. In order to explain the high stress exponent observed in this study, a threshold stress analysis was performed. Li and Langdon [43,44] have previously proposed that the threshold stress value, σ_{th}, can be determined by extrapolating the double logarithmic line of the minimum creep rate versus stress to a value of $10^{-10}\,s^{-1}$. In the case of the Y2 alloy, this method yielded threshold stress values of 147.29 MPa at 150 ℃, 94.52 MPa at 175 ℃, and 76.99 MPa at 200 ℃. Fig. 13(b) illustrates the relationship between the steady-state creep rate and the normalized effective stress (σ_e=σ-σ_{th}) of the Y2 alloy on a logarithmic coordinate axis. By taking into account the threshold stress, the recalculated creep stress index falls within a reasonable range, ranging from 1.6 to 1.9. This adjustment helps to bring the stress exponent values into alignment with the expected values.

5. Conclusions

The influence of the content of LPSO phase, temperature, and applied stress on the creep behavior of LPSO-containing Mg-Y-Zn alloys was studied through high-temperature creep experiments. The creep activation energy (Q_c) and creep stress index (n) of the Mg-LPSO alloy under different applied stresses were obtained through creep constitutive equations. The main conclusions are reached as follows:

(1) The influence of LPSO phases on the creep resistance of Mg-Y-Zn alloys exhibits temperature-dependent trends. Below 200 °C, LPSO phases have a negligible influence on creep resistance. However, at higher temperatures (>200 °C), the presence of LPSO phases accelerates creep deformation. The alloy with a higher LPSO content correlates with a reduction in creep resistance. This trend suggests a temperature-driven transition in the role of LPSO phases during creep deformation.

(2) At 300 °C, LPSO phases promote an increase in the creep rates, particularly in the early stages of deformation. However, their influence diminishes in the later creep stages as deformation is increasingly governed by diffusion-assisted mechanisms.

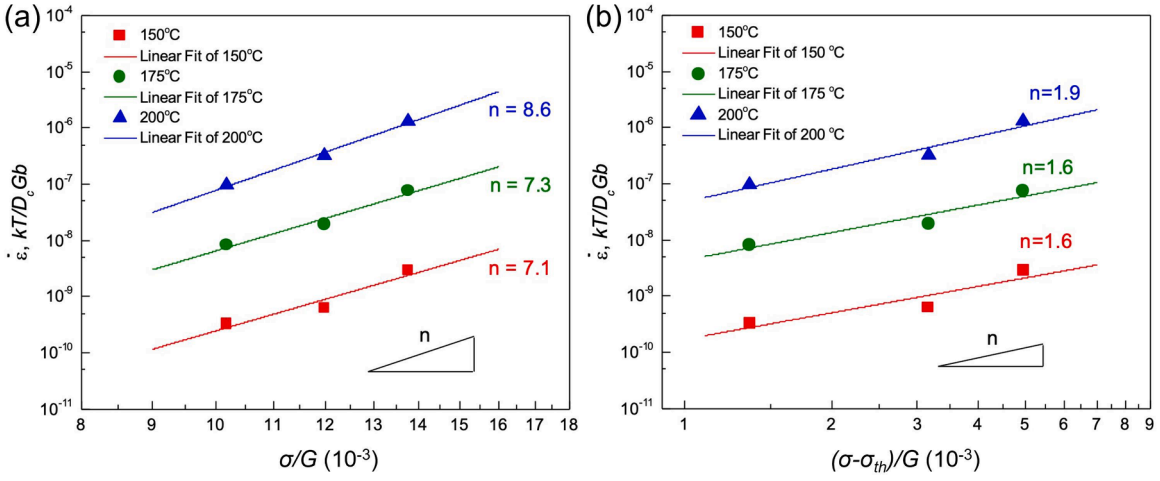

Fig. 13. Normalized creep rate versus normalized stress according to Mukherjee-Bird-Dorn equation (a) and normalized minimum creep rate plotted against normalized effective stress ($(\sigma-\sigma_{th})/G$) at different temperatures (b) for the Y2 alloy.

Superplasticity was observed under high-temperature creep conditions, attributed to the enhanced diffusion of solute atoms along the stacking faults within the LPSO structures, facilitating grain boundary sliding and stress relaxation.

(3) The creep behavior of Mg-LPSO alloys follows power-law creep within the 150–200 °C temperature range and under 170–230 MPa stress conditions. The creep constitutive equation reveals a high stress exponent (7.1–8.6) and a relatively low activation energy (80.98–90.63 $kJ \cdot mol^{-1}$), indicating a threshold stress mechanism. This mechanism arises from the load transfer effect between the Mg matrix and the LPSO phase, which resists deformation at lower temperatures but becomes less effective as temperature increases. The corrected creep stress exponent further suggests a transition from dislocation-controlled creep to diffusional creep as the dominant deformation mechanism at elevated emperatures.

CRediT authorship contribution statement

Wang Jie: Writing – original draft, Investigation. **Zhu Gaoming:** Writing – review & editing, Investigation, Funding acquisition. **Wang Dandan:** Writing – review & editing, Investigation, Funding acquisition. **Liu Yahui:** Methodology. **Zeng Xiaoqin:** Supervision, Resources, Funding acquisition. **Knezevic Marko:** Writing – review & editing.

Declaration of Competing Interest

The authors declare that they have no known competing financial interests or personal relationships that could have appeared to influence the work reported in this paper.

Acknowledgements

The authors wish to acknowledge the financial support of the National Natural Science Foundation of China (Nos. 52425101 and 52301018), Natural Science Foundation of Jiangsu Province (No. BK20220627). We acknowledge DESY (Hamburg, Germany), a member of the Helmholtz Association HGF, for the provision of experimental facilities. Parts of this research were carried out at the PETRA III beamline P21.2.

Appendix A. Supporting information

Supplementary data associated with this article can be found in the online version at doi:10.1016/j.jallcom.2025.180110.

Data Availability

Data will be made available on request.

References

[1] A.A. Luo, A.K. Sachdev, Applications of Magnesium Alloys in Automotive Engineering. Adv. Wrought Magnes. Alloy, Elsevier, 2012, pp. 393–426.
[2] T. Xu, Y. Yang, X. Peng, J. Song, F. Pan, Overview of advancement and development trend on magnesium alloy, J. Magnes. Alloy 7 (2019) 536–544.
[3] K. Maruyama, M. Suzuki, H. Sato, Creep strength of magnesium-based alloys, Metall. Mater. Trans. A. 33 (2002) 875–882.
[4] J.A. Del Valle, O.A. Ruano, Separate contributions of texture and grain size on the creep mechanisms in a fine-grained magnesium alloy, Acta Mater. 55 (2007) 455–466.
[5] T. Chen, Q. Huo, S. Hu, C. Wang, Y. Zhang, Z. Zhang, S. Li, X. Yang, Tracing the effects of calcium, stannum, and zinc additions on the creep resistance of Mg–Al-based alloys, Metall. Mater. Trans. A. 54 (2023) 2730–2743.
[6] T. Mineta, H. Saijo, S. Shibata, S. Nakaya, H. Sato, Transition of superplastic and dislocation creep of duplex Mg–Li–Al–Zn alloy, Mater. Sci. Eng. A. 886 (2023) 145714.
[7] Z. Xiao, Q. Huo, Y. Zhang, Z. Zhang, Z. Li, A. Hashimoto, X. Yang, Tensile creep anisotropy of a Mg-2Y alloy extruded sheet with a splitted texture, J. Alloy. Compd. 823 (2020) 153754.
[8] B.L. Mordike, Creep-resistant magnesium alloys, Mater. Sci. Eng. A. 324 (2002) 103–112.
[9] N. Mo, I. McCarroll, Q. Tan, A. Ceguerra, Y. Liu, J. Cairney, H. Dieringa, Y. Huang, B. Jiang, F. Pan, M. Bermingham, M.X. Zhang, Understanding solid solution strengthening at elevated temperatures in a creep-resistant Mg–Gd–Ca alloy, Acta Mater. 181 (2019) 185–199, https://doi.org/10.1016/j.actamat.2019.09.058.
[10] J. Li, J. Wu, L. Jin, M. Celikin, F. Wang, S. Dong, J. Dong, The role of dislocation-solute interactions on the creep behaviour of binary Mg–RE alloys, Sci. Rep. 11 (2021) 2860, https://doi.org/10.1038/s41598-021-82517-5.
[11] J. Wang, L. Wang, G. Zhu, B. Zhou, T. Ying, X. Zhang, Q. Huang, Y. Shen, X. Zeng, H. Jiang, Understanding the high strength and good ductility in LPSO-containing Mg alloy using synchrotron X-ray diffraction, Metall. Mater. Trans. A. 49 (2018) 5382–5392.
[12] J. Wang, G. Zhu, L. Wang, X. Zhang, M. Knezevic, X. Zeng, Strengthening mechanisms, hardening/softening behavior, and microstructure evolution in an LPSO magnesium alloy at elevated temperatures, Mater. Charact. (2023) 113066.
[13] E. Oñorbe, G. Garcés, F. Dobes, P. Pérez, P. Adeva, High-temperature mechanical behavior of extruded Mg-Y-Zn alloy containing LPSO phases, Metall. Mater. Trans. A. 44 (2013) 2869–2883.
[14] D. Xu, E. Han, Y. Xu, Effect of long-period stacking ordered phase on microstructure, mechanical property and corrosion resistance of Mg alloys: A review, Prog. Nat. Sci. Mater. Int. 26 (2016) 117–128.
[15] G. Garcés, E. Oñorbe, F. Dobes, P. Pérez, J.M. Antoranz, P. Adeva, Effect of microstructure on creep behaviour of cast Mg97Y2Zn1 (at%) alloy, Mater. Sci. Eng. A. 539 (2012) 48–55.
[16] E. Oñorbe, G. Garcés, P. Pérez, P. Adeva, Effect of the LPSO volume fraction on the microstructure and mechanical properties of Mg–Y2X–ZnXalloys, J. Mater. Sci. 47 (2012) 1085–1093, https://doi.org/10.1007/s10853-011-5899-4.
[17] T. Mineta, D. Takahashi, W. Bando, H. Sato, K. Hagihara, M. Yamasaki, Creep deformation behavior and microstructure of α-Mg/long-period stacking ordered (LPSO) duplex Mg-Y-Zn alloy prepared by hot extrusion and heat treatment, Mater. Today Commun. 39 (2024) 108912, https://doi.org/10.1016/j.mtcomm.2024.108912.
[18] G. Zhu, L. Wang, J. Wang, J. Wang, J.S. Park, X. Zeng, Highly deformable Mg–Al–Ca alloy with Al_2Ca precipitates, Acta Mater. 200 (2020) 236–245, https://doi.org/10.1016/J.ACTAMAT.2020.09.006.
[19] A.K. Mukherjee, An examination of the constitutive equation for elevated temperature plasticity, Mater. Sci. Eng. A. 322 (2002) 1–22.
[20] J. Wang, G. Zhu, L. Wang, Q. Zhu, E. Vasilev, X. Zeng, M. Knezevic, Dislocation-induced plastic instability in a rare earth containing magnesium alloy, Materialia 15 (2021) 101038, https://doi.org/10.1016/J.MTLA.2021.101038.
[21] J. Wang, J. Zhang, X. Zong, C. Xu, Z. You, K. Nie, Effects of Ca on the formation of LPSO phase and mechanical properties of Mg-Zn-Y-Mn alloy, Mater. Sci. Eng. A. 648 (2015) 37–40, https://doi.org/10.1016/j.msea.2015.09.046.
[22] F.C. Campbell, Elements of metallurgy and engineering alloys, ASM international, 2008.
[23] Y. Li, T.G. Langdon, A comparison of the creep properties of an Al-6092 composite and the unreinforced matrix alloy, Metall. Mater. Trans. A. 29 (1998) 2523–2531.
[24] Z. Tobolová, J. Čadek, An interpretation of steady state creep, Philos. Mag. 26 (1972) 1419–1428.
[25] H.R. Erfanian-Naziftoosi, E.J. Rincón, H.F. López, Creep properties of the as-cast Al-A319 alloy: T4 and T7 heat treatment effects, Metall. Mater. Trans. A. 47 (2016) 4258–4267.
[26] A.N. Campbell, S.S. Tsao, D. Turnbull, The effect of Au and Ag additions on the power-law creep behavior of Pb, Acta Met. 35 (1987) 2453–2464.
[27] J. Combronde, G. Brebec, Anisotropie d'autodiffusion du magnesium, Acta Met. 19 (1971) 1393–1399.
[28] M. Suzuki, T. Kimura, J. Koike, K. Maruyama, Effects of zinc on creep strength and deformation substructures in Mg–Y alloy, Mater. Sci. Eng. A. 387 (2004) 706–709.
[29] S.K. Das, Y.-B. Kang, T. Ha, I.-H. Jung, Thermodynamic modeling and diffusion kinetic experiments of binary Mg–Gd and Mg–Y systems, Acta Mater. 71 (2014) 164–175.
[30] M.E. Kassner, Fundamentals of creep in metals and alloys, Butterworth-Heinemann, 2015.
[31] D.D. Yin, Q.D. Wang, C.J. Boehlert, V. Janik, Y. Gao, W.J. Ding, Creep behavior of Mg–11Y–5Gd–2Zn–0.5 Zr (wt%) at 573 K, Mater. Sci. Eng. A. 546 (2012) 239–247.
[32] T.G. Langdon, Creep at low stresses: An evaluation of diffusion creep and Harper-Dorn creep as viable creep mechanisms, Metall. Mater. Trans. A. 33 (2002) 249–259.
[33] M. Celikin, M. Pekguleryuz, The role of α-Mn precipitation on the creep mechanisms of Mg–Sr–Mn, Mater. Sci. Eng. A. 556 (2012) 911–920.
[34] M. Pekguleryuz, M. Celikin, Creep resistance in magnesium alloys, Int. Mater. Rev. 55 (2010) 197–217.
[35] H. Somekawa, K. Hirai, H. Watanabe, Y. Takigawa, K. Higashi, Dislocation creep behavior in Mg–Al–Zn alloys, Mater. Sci. Eng. A. 407 (2005) 53–61.
[36] H. Luthy, A.K. Miller, O.D. Sherby, The stress and temperature dependence of steady-state flow at intermediate temperatures for pure polycrystalline aluminum, Acta Met. 28 (1980) 169–178.
[37] H. Mecking, Y. Estrin, The effect of vacancy generation on plastic deformation, Scr. Met. 14 (1980) 815–819.
[38] M.E. Kassner, J. Pollard, E. Evangelista, E. Cerri, Restoration mechanisms in large-strain deformation of high purity aluminum at ambient temperature and the determination of the existence of "steady-state, Acta Metall. Mater. 42 (1994) 3223–3230.
[39] S. Sandlöbes, M. Friák, S. Zaefferer, A. Dick, S. Yi, D. Letzig, Z. Pei, L.F. Zhu, J. Neugebauer, D. Raabe, The relation between ductility and stacking fault energies

in Mg and Mg-Y alloys, Acta Mater. 60 (2012) 3011–3021, https://doi.org/10.1016/j.actamat.2012.02.006.
[40] C. Praveen, J. Christopher, V. Ganesan, G.V.P. Reddy, G. Sasikala, S.K. Albert, Constitutive modelling of transient and steady state creep behaviour of type 316LN austenitic stainless steel, Mech. Mater. 137 (2019) 103122.
[41] J.A. del Valle, O.A. Ruano, Critical analysis of threshold stresses in the creep mechanisms of a powder metallurgy magnesium alloy AZ31, Metall. Mater. Trans. A. 51 (2020) 2344–2358.
[42] S.-M. Zhu, M.A. Gibson, M.A. Easton, J.-F. Nie, The relationship between microstructure and creep resistance in die-cast magnesium–rare earth alloys, Scr. Mater. 63 (2010) 698–703.
[43] A. Srinivasan, H. Dieringa, C.L. Mendis, Y. Huang, R.R. Kumar, K.U. Kainer, N. Hort, Creep behavior of Mg–10Gd–xZn (x= 2 and 6 wt%) alloys, Mater. Sci. Eng. A. 649 (2016) 158–167.
[44] Y. Li, T.G. Langdon, A simple procedure for estimating threshold stresses in the creep of metal matrix composites, Scr. Mater. 36 (1997) 1457–1460.